ACS APPLIED MATERIALS & INTERFACES

Research Article

www.acsami.org

Optimization and Stabilization of Electrodeposited Cu_2ZnSnS_4 Photocathodes for Solar Water Reduction

Lorenzo Rovelli,[†] S. David Tilley,[‡] and Kevin Sivula*[,†]

[†]Laboratory for Molecular Engineering of Optoelectronic Nanomaterials and [‡]Laboratory of Photonics and Interfaces, Institute of Chemical Sciences and Engineering, École Polytechnique Fédérale de Lausanne, Station 6, CH-1015 Lausanne, Switzerland

Supporting Information

ABSTRACT: Cu_2ZnSnS_4 (CZTS) is a promising p-type semiconductor that has not yet been extensively investigated for solar fuel production via water splitting. Here, we optimize and compare two different electrodeposition routes (simultaneous and sequential) for preparing CZTS electrodes. More consistent results are observed with the simultaneous route. In addition, the effect of etching and the presence of a CdS buffer layer on the photocurrent are investigated. Finally, we demonstrate for the first time the stabilization of these electrodes using protecting overlayers deposited by atomic layer deposition (ALD). Our best performing protected electrodes (Mo/CZTS/CdS/AZO/TiO_2/Pt) exhibited a photocurrent of over 1 mA cm^{-2} under standard one sun illumination conditions and a significant improvement in stability over unprotected electrodes.

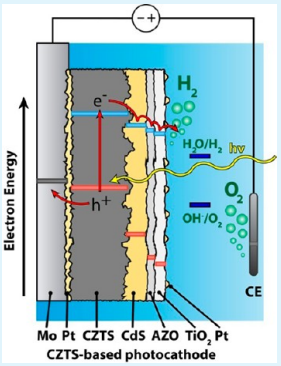

KEYWORDS: *photoelectrochemical, CZTS, ALD, protecting overlayers, water splitting, hydrogen*

1. INTRODUCTION

Inexpensive and efficient routes to the chemical storage of solar energy are urgently needed for a sustainable energy economy. Hydrogen fuel is a promising candidate as a renewable energy vector,[1] and an elegant and potentially the most efficient approach to solar hydrogen production is the direct conversion of sunlight using a water splitting photoelectrochemical (PEC) cell that employs a direct semiconductor−liquid interface.[2,3] Numerous semiconductor materials and cell configurations have been investigated for PEC water splitting in the last decades,[4] and a tandem cell approach has emerged as a promising route that can both generate sufficient photopotential for water splitting and harvest a significant portion of the solar spectrum.[5] In particular, a dual absorber (D4-type) photoanode/photocathode tandem device is reasonably simple to construct and could achieve solar-to-chemical efficiencies over 20% when using optimized absorber band gap energies even with large assumed losses.[6]

While much attention has been devoted to photoanode materials,[7] the identification of stable and inexpensive p-type photocathode materials currently limits the development of the PEC tandem cell. P-type silicon has been extensively investigated as a candidate material;[8,9] however, its band gap energy, E_g, of 1.1 eV is lower than optimum for the generation of sufficient photovoltage in a two-electrode D4 tandem cell (where a bottom cell with E_g = 1.3−1.4 is ideal when reasonable losses are considered).[6] Tunable band gap systems, like III−V semiconductors such as $GaInP_2$, can be optimized to act as highly efficient photocathode materials in D4 tandem cells for water splitting.[10] However, for a commercially viable PEC device, the overall solar-to-chemical conversion efficiency is far from being the only important parameter: indeed, other crucial features are the stability of the device, a device composition comprising inexpensive and readily available materials, and a manufacturing process employing easily scalable, reproducible, and economical techniques. Indeed, copper oxide-based materials, such as Cu_2O, have gained significant interest as they consist of common atoms and can be electrodeposited in relatively mild conditions,[11] but their E_g in the range of 2.0−2.2 eV limits their solar light absorption and excludes them from operating in tandem with common photoanode materials such as Fe_2O_3 (E_g = 2.1 eV).[12] Chalcopyrite-type materials, exemplified by $CuIn_xGa_{1-x}Se$ (CIGS), are Cu-based materials that offer reduced band gap energies compared to Cu_2O and thus higher potential solar conversion efficiency. CIGS has recently shown promising activity as a PEC photocathode.[13,14] However, as is the case for $GaInP_2$, the scarcity and the very high demand of indium make this material increasingly expensive and therefore less relevant for energy production at the scale of global demand.

An emergent material sharing many properties with CIGS is Cu_2ZnSnS_4 (CZTS). This material is structurally similar to CIGS and has a direct band gap of ca. 1.5 eV,[15] which is ideally suited for the bottom cell in a D4 PEC tandem cell. In addition, CZTS is composed of only inexpensive and readily available elements, since indium and gallium are replaced by zinc and tin,

Received: May 31, 2013
Accepted: July 31, 2013
Published: August 14, 2013

which makes it very attractive in view of large scale applications. While CZTS has been extensively investigated for use in photovoltaic cells, it is only in the last five years that the first investigations of the photoelectrochemical properties of this material have been carried out. In most of the cases, however, these investigations have been performed using sacrificial agents (such as Eu^{3+}) in an effort to further characterize its photovoltaic properties rather than for solar fuel production.[16−19] The PEC properties of cosputtered CZTS films were investigated for the first time under water-splitting conditions in 2010.[20] The reported photocurrents were remarkable, but the stability of the cells was poor. The recent development of strategies to stabilize photocathode materials for PEC water reduction[11,21] motivated our investigation of this promising material for PEC energy conversion. Herein, we report CZTS photocathodes prepared by inexpensive and scalable electrodeposition techniques applied for photoelectrochemical water reduction. We compare two variations on the electrodeposition of precursor films and investigate the roles of the different layers included on the photoactivity. We further demonstrate, for the first time, the ability to improve and stabilize the photocurrent delivered by CZTS electrodes by protecting their surface using atomic layer deposition overlayers.

2. EXPERIMENTAL SECTION

The general approach toward the fabrication of CZTS electrodes was the sulfurization of electro-deposited precursors. The CZTS-precursor was electrodeposited on a molybdenum foil following two different routes: in the first route, adapted from previous work carried out by Araki et al.,[22] zinc, tin, and copper were simultaneously deposited from the same bath (codeposition). In the second strategy, inspired by work published by Ma et al.,[23] the metals were sequentially deposited in the order Cu−Sn−Zn from three separate baths, to form a stacked metallic layer. Overall, ca. 60 electrodeposited CZTS samples were prepared of which about 35 were sequential and 25 were simultaneous.

Simultaneous Electrodeposition. The composition of the bath solution for the simultaneous deposition was as follows: 20 mM of $CuSO_4$ anhydrous, 200 mM of $ZnSO_4{\cdot}7H_2O$, 10 mM of hydrated $SnCl_2$, and 500 mM of trisodium citrate. The electrodeposition from ca. 160 mL of this solution was carried out at room temperature under stirring in potentiostatic conditions with a 3-electrode cell with a platinum mesh used as counter electrode and an Ag/AgCl reference electrode. Typically, the potential was kept at −1.15 V vs Ag/AgCl for 20 min, although other durations and potentials were tried as well.

Sequential Electrodeposition. The conditions for sequential electrodeposition were adapted from ref. 23 in order to deposit the metals from stable and clear solutions. The compositions of the solution baths for the sequential electrodeposition were the following: 0.01 M $CuCl_2{\cdot}2H_2O$, pH 3.0 for the copper solution; 0.013 M $SnCl_2$, pH 2.0 or 13.0 for the tin solution; 0.04 M $ZnSO_4{\cdot}7H_2O$, pH 11.0 for the zinc solution. The electrodeposition from ca. 200 mL of these solutions was carried out at room temperature under stirring in potentiostatic conditions with a 3-electrode configuration. A platinum mesh was used as counter electrode, while the reference electrode was Ag/AgCl. The applied potentials vs Ag/AgCl were the following: −0.50 V for copper deposition, −1.10 V for tin deposition, and −1.30 V for zinc deposition. The durations of electrodeposition were adjusted according to the current density, in order to achieve an overall charge of 1.0, 0.7, and 0.6 C cm^{-2} for copper, tin, and zinc, respectively. Additional details including substrate preparation and solution preparation for both electrodepositing techniques are provided in the Supporting Information.

Sulfurization. After electrodeposition, the electrodes were heated under argon in the presence of elemental sulfur in a tube furnace at 585−600 °C for 1 h. The sequentially deposited electrode was first annealed at 350 °C for 30 min to amalgamate the three layers. Complete details are included in the Supporting Information.

Etching. Some samples were subjected to an etching step after sulfurization. In these cases, the CZTS thin films were dipped for 1 min in a 0.1 M KCN solution at 55 °C immediately before the next step of CdS deposition or atomic layer deposition.

CdS Deposition. The effect of a CdS overlayer was also examined on the CZTS electrodes. The CdS was deposited by the solution-based chemical bath deposition (CBD) technique using $Cd(CH_3COO)_2$ solutions in water as described in the Supporting Information. The electrodes were immersed in the bath solution at 75 °C and kept for 5 min under mild stirring. The surface of the sample was then thoroughly rinsed with water, air-dried, and finally annealed in air at 200 °C for 30 min.

Protective Overlayer Deposition. Electrodes were protected with an overlayer of aluminum-doped zinc oxide (AZO) and one of titanium dioxide using atomic layer deposition (ALD) following the procedure reported previously.[11] In brief, the ALD was carried out at a substrate temperature of 150 °C. AZO was deposited by running 1 cycle of trimethyl aluminum and water after 20 cycles of diethyl zinc and water. Titanium dioxide (TiO_2) was deposited using tetrakis-(dimethylamino)titanium (TDMAT) and water as the Ti and O precursors, respectively. Each precursor was held in the chamber for 2.0 s followed by a 15.0 s nitrogen purge. All of the ALD precursors were kept at room temperature during deposition, except for TDMAT, which was kept at 75 °C. Additional details including growth rates are reported in the Supporting Information.

Electrochemical Characterization. Prior to photoelectrochemical characterization, the surface of the samples has been further modified by electrodeposition of a hydrogen evolution reaction (HER) catalyst (platinum) using standard techniques detailed in the Supporting Information. The photoelectrochemical properties of the CZTS electrodes were characterized in a 3-electrode PEC cell with an exposed area of 0.283 cm^2. Two aqueous electrolytes have been employed for photoelectrochemical measurements: one was a pH 7.0 phosphate buffer solution (0.5 M). The second was a 0.1 M Na_2SO_4 solution, with the pH adjusted to 9.0 by addition of NaOH. Only minor differences were observed between the performance of the electrodes in the two electrolytes. A platinum wire was used as counter electrode, while the reference electrode was a Ag/AgCl sat. KCl electrode equipped with a salt bridge. The performances of the samples were evaluated under chopped light illumination by linear sweep voltammetry and galvanostatic experiments. The light source was a 450W Xe lamp (Osram) equipped with an infrared filter (KG3 filter, 3 mm, Schott) and calibrated with a Si photodiode to simulate AM1.5 illumination (100 mW cm^{-2}). The scan rate for linear sweep voltammetry was 10 mV s^{-1}, and the potential was swept from anodic to cathodic potentials, unless otherwise stated. Electrochemical impedance spectroscopy measurements were performed in the dark under the same conditions as linear sweep measurements. The frequency range selected was between 0.1 and 10^5 Hz, and an AC perturbation of 10 mV was applied. Different potentials were applied with steps of 15−20 mV and an equilibration time of 10 s after changing the applied potential. Cyclic voltammetry (CV) was performed in the dark and under illumination to test the electrochemical stability of the electrodes with and without protecting layers. The potential was typically swept at a rate of 10 mV s^{-1} for the CV experiments.

Other Characterization. The CZTS electrodes were characterized by scanning electron microscopy (SEM), X-ray diffraction (XRD), and UV−vis-NIR reflectance spectroscopy. The morphology of the films was characterized using a scanning electron microscope (FEI, XL30-FEG); the acceleration voltage was 10.0 kV. X-ray diffraction patterns were acquired with a Bruker D8 Discover diffractometer in locked coupled mode, using Cu Kα radiation (1.540598 Å) and a Ni β-filter. Spectra were acquired with a linear silicon strip "Lynx Eye" detector from 2θ = 15°−60° at a scan rate of 5° min^{-1}, an increment of 0.02°, and a source slit width of 1 mm. The optical properties of the thin films were characterized by reflectance spectroscopy using a Shimadzu UV-3600 UV−vis-NIR spectrometer equipped with a 60 mm integrating sphere. KBr was used as "white standard" reference. The optical band gap of the materials was estimated by Tauc analysis after

Kubelka–Munk transformation of the total reflectance. Other characterization techniques (e.g., Raman spectroscopy and IPCE measurement) are described in the Supporting Information.

3. RESULTS AND DISCUSSION

The ability to deposit CZTS by electrochemical routes has important advantages. In addition to being a well-established low-temperature, scalable, and inexpensive technique compared to other solution-based techniques, electroplating is also particularly environmentally friendly since it avoids usage of organic solvents and of toxic or dangerous reagents (in contrast to recently developed hybrid-slurry approaches for the preparation of CZTS, which involve the use of hydrazine).[24] Two different strategies toward the preparation of CZTS thin films by electrodeposition, sequential[23] and simultaneous electrodeposition,[22] were thus extensively investigated for this work. A few general conclusions can be drawn from the comparison of these approaches. The sequential deposition of the metals is more time-consuming and cumbersome and therefore less interesting for industrial application but potentially allows for more precise stoichiometric tuning compared to the simultaneous deposition method. Indeed, the simultaneous electrodeposition of three metals in the correct ratios is expected to be very sensitive to the concentrations and the applied potentials. However, despite the fact that more effort was devoted in this work to the study of the sequential approach, the best results were obtained with the simultaneous approach. To the best of our knowledge, this method has never been applied previously for PEC water splitting. Overall, the simultaneous deposition approach was qualitatively superior in terms of film morphology, photoactivity of the photoelectrode, and especially in terms of reproducibility of the method. Despite all efforts to carefully reproduce the fabrication procedure for each of the samples, the sequentially electrodeposited coating often appeared visually different from one deposition to the next. We attribute this variability to a poor adhesion of the deposited metals on the underlying substrate. In the original report of this strategy, this drawback was not mentioned; however, a molybdenum mesh was used as a substrate instead of the more common Mo foil. In our case, the surface of even the best performing sequentially prepared films appeared to feature many pinholes and the coverage was far from homogeneous. The thin-film morphology after sulfurization is shown in Figure 1a where islands of material can be seen on the Mo substrate. The simultaneously deposited CZTS electrodes after sulfurization (Figure 1b) exhibited a film with features of a similar dimension. However, in contrast to the sequentially prepared films, the coating was continuous, compact, and pinhole-free as can be seen by the inset in Figure 1b which shows a flake of the film detached from the substrate underneath.

The typical XRD spectrum obtained with sequential deposition exhibited weak reflection signals compared to films of similar thickness prepared by the simultaneous approach suggesting that much of the deposited material was amorphous (Figure 2a). Because of the poor and less reproducible results with the sequential technique, the optimization of various parameters for the preparation of the photoelectrodes was difficult to achieve systematically.

On the contrary, for the simultaneous deposition, the procedure was much simpler and much more reproducible, allowing for easier optimization of various parameters in the synthesis of CZTS and its post-treatments. In addition, the

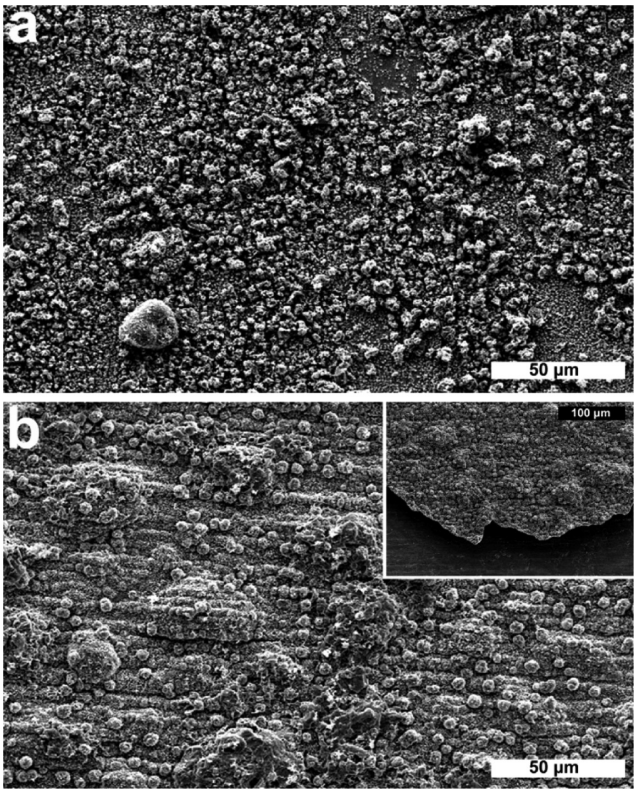

Figure 1. Scanning electron micrograph of the (a) sequentially and (b) simultaneously deposited CZTS films after electrode deposition and sulfurization. The inset of (b) shows a flake of the film which had been partially detached from the Mo substrate.

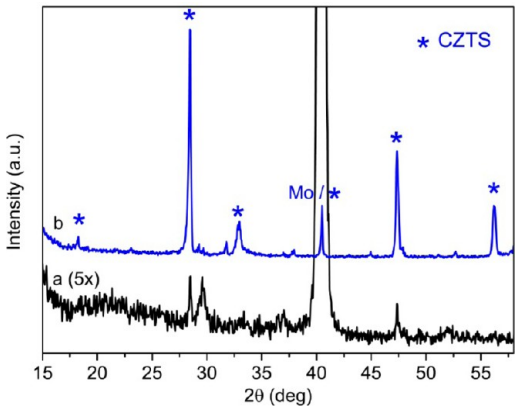

Figure 2. XRD patterns of the as-sulfurized sequentially (a) and simultaneously (b) deposited CZTS films. Note that the spectrum is stretched by a factor of 5 in the vertical direction for (a). Reflections from the CZTS kesterite phase and the molybdenum substrate are indicated.

XRD data (Figure 2b) revealed strong reflections from the kesterite CZTS phase and only minor impurity peaks. Since it is known that common secondary phases have peaks which overlap with those of the kesterite phase,[25] Raman spectroscopy was also performed on simultaneously deposited sample after sulfurization (Figure S1, Supporting Information). In addition to the characteristic peaks from CTZS (290 and 340 cm^{-1}),[26,27] MoS_2 (at 380 and 410 cm^{-1})[27] from the substrate and impurity phases of copper and zinc sulfides were seen. The

presence of these impurities will be discussed further in reference to the KCN etching.

The results of UV−vis-NIR diffuse reflectance measurements of as-sulfurized CZTS films support the conclusions drawn from the above results. Tauc plots (Figure S2, Supporting Information) of the samples prepared by sequential deposition typically showed an onset of absorption beginning around 1.0 eV, this feature appeared to be very reduced for the samples which were made by simultaneous deposition. We attribute this feature to the presence of secondary phases of the type Cu_xS_y that indeed exhibit a band gap energy of around 1.0 eV.[28] On the other hand, the absorption band showing an onset around 1.4 eV (attributable to CZTS) is distinct for the simultaneously deposited films and barely visible for the sequentially deposited film.

To estimate the valence band-edge of the electrodeposited CZTS material, the flat-band potential has been determined using the Mott−Schottky method. The flat-band potential was found to be similar for the two deposition routes and was between 0.6 and 0.7 V vs RHE at pH 5 (Figure S3, Supporting Information). The value for the simultaneously deposited sample was slightly cathodically shifted, by ca. 50 mV, with respect to the sequentially deposited sample. For comparison, using a similar electrodeposition route, Scragg et al. reported a value of 0.20 V vs Ag/AgCl at pH 2.3, corresponding to approximately 0.54 V vs RHE, using the photocurrent onset potential.[16] By considering the value of the flat-band potential as a coarse approximation for the valence band edge, one can estimate the conduction band edge of the material by adding the value of the optical band gap to the latter. With this coarse approximation, it can be concluded that both electrodeposition routes lead to materials where the driving force for water reduction exceeds 0.7 V at pH 5 and is therefore expected to be sufficient for a wide range of pH conditions around this value.

In terms of photoactivity toward hydrogen evolution from aqueous solutions, determined by linear sweep voltammetry under chopped light illumination (AM 1.5 G 100 mW cm^{-2}), the as-sulfurized CZTS films showed very limited activity regardless of the electrodeposition route and the difference in the photoactivity between the two routes did not appear to be appreciable. In both cases, the photocurrent generated was on the order of 1 μA cm^{-2} at 0 V vs RHE, while the dark current was on the order of hundreds of microamperes per square centimeter. Interestingly, a dramatic improvement was obtained by etching the samples in a KCN solution after sulfurization. This procedure was extensively investigated by Scragg et al.[29,30] but not mentioned in the reports by Ma et al.[23] and Araki et al.[22] The treatment has been reported to preferentially etch secondary phases from the surface of the film. Indeed, Raman spectroscopy of a simultaneously deposited sample before and after the etching (Figure S1, Supporting Information) shows the decrease in both the peaks corresponding to the ZnS (345 cm^{-1})[27] and the Cu_xS_y (475 cm^{-1})[26] after the etching step. In addition, the etching step has a remarkable effect on the dark current of the electrode. For the sequentially deposited electrode, approximately a 10-fold increase in the photocurrent and almost a 10-fold decrease in the dark current was observed (Figure 3a). The etching procedure also showed improvement for the simultaneously deposited electrode, although less dramatic (not shown), and as such, the etching procedure was used for the remainder of the work.

Despite the improvement offered by the KCN etching step to the photoelectrodes for water reduction, the photoactivity of

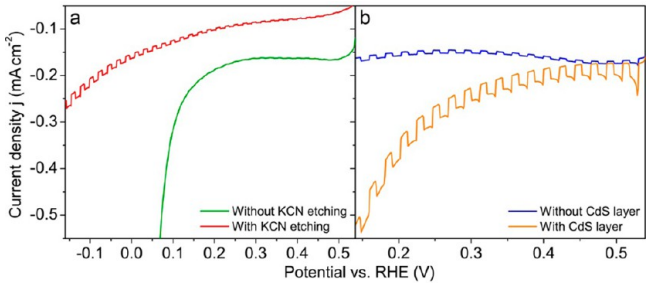

Figure 3. The effect of additional treatments on the photoelectrochemical performance are shown by linear sweep voltammograms for sequentially deposited CZTS electrodes showing the influence of KCN etching (a) and of the CdS layer (b). Scans were recorded at pH 9 under chopped illumination.

the etched CZTS thin films was still very moderate, on the order of tens of microamperes per square centimeter. This is perhaps expected given that the deposition of a suitable n-type material on top of CZTS is typically employed to promote charge separation and in turn hinder recombination of the photogenerated charge carriers. The material most often employed for this purpose is CdS. However, given that our ultimate goal of this work is to protect the CZTS with an overlayer to afford stability and that the (n-type) AZO/TiO_2 combination already reported has been speculated to aid charge extraction in Cu_2O,[21] we hoped to show that a CdS layer was not necessary on these electrodes for water reduction. In order to properly compare, we first prepared the standard n-CdS overlayer. Upon the chemical bath deposition of n-CdS on top of the CZTS layer, the photocurrent generated by the cell was indeed 5 to 10 times higher for both of the deposition approaches (this effect is shown for the sequential deposition approach in Figure 3b). This however led to a significant increase in the dark current and to an even more dramatic decrease in the stability of the photoelectrode: the photocurrent clearly appears to decrease during the linear sweep (hence within seconds), despite the fact that the sweep was carried out from higher to lower potentials. The same behavior was observed for the simultaneously deposited electrodes as well. This lack of stability, which was present regardless of the deposition approach and even after deposition of a hydrogen evolution reaction (HER) catalyst (platinum) on the surface of the film, clearly indicates that the photogenerated electrons and holes ultimately lead to the deactivation of the CZTS/CdS electrode (e.g by photocorrosion reactions), instead of contributing to hydrogen evolution.

The critical issue of electrode photocorrosion was next overcome by protection of the CZTS-based photoelectrode through the atomic layer deposition of conformal AZO and TiO_2 layers a few nanometers in thickness. This material combination has been shown in similar systems to form a type-II (or staggered) band alignment (such as in combination with p-type Cu_2O),[21] which contributes to active charge separation and also retains enough driving force for the hydrogen evolution reaction (HER) to occur. ALD also offers conformal and pinhole-free coverage that can prevent the direct contact of the protected material with the electrolyte using only a few nanometers of overlayer.

To protect the CZTS-based electrodes, overlayers of AZO and TiO_2 (20 and 50 nm, respectively) were added using a previously developed recipe.[21] No significant change in morphology was observed by SEM upon the deposition as

shown in Figures S4 and S5, Supporting Information. For the Mo/CZTS/CdS electrodes, the protecting strategy yielded a significant improvement in the photocurrent. Figure 4a shows

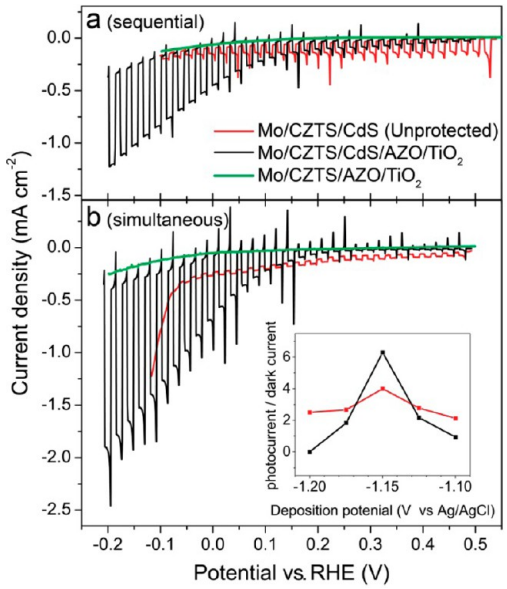

Figure 4. Linear sweep voltammograms under chopped light illumination for the sequentially (a) and simultaneously (b) deposited CZTS-based films, with and without the ALD protective layer (AZO/TiO_2) or the CdS layer. All measurements were carried out at pH 7. The inset of (b) shows the photoactivity (expressed as the ratio of photocurrent to dark current) of the CZTS/CdS cells as a function of the potential applied during simultaneous electrodeposition. Photoactivity was assessed by linear sweep voltammetry: current values were taken at 0.2 V vs Ag/AgCl at pH 9 for unprotected samples (for stability reasons) and at 0 V vs RHE at pH 7 for protected samples.

this for the case of the sequential deposition route. The photocurrent of the unprotected Mo/CZTS/CdS electrode (red curve) was typically lower than 0.1 mA cm^{-2} at 0 V vs RHE, and the photocurrent decreased as the potential was scanned cathodically due to the electrode deactivation. However, the activity after ALD deposition showed a 5-fold increase, to over 0.5 mA cm^{-2} for the best performing sample, and the photocurrent increased with increasing cathodic potential, as expected for p-type behavior. We note that the average performance of multiple samples prepared at these conditions was 0.15 mA cm^{-2} at 0 V vs RHE, indicating a significant variability.

The effect of the protecting layers is even more striking for the case of the simultaneous deposition approach: here again, due to the poor stability of the photoelectrode, the photocurrent appeared to strongly decrease during the course of the measurement for the Mo/CZTS/CdS electrode (and typically was much lower than 0.1 mA at RHE), as shown in Figure 4b (red curve). Given the rapid deactivation of the unprotected electrodes in Figure 4a,b, the comparison of the photocurrent magnitudes of these samples is not possible. However, similar to the sequentially deposited electrode, the photocurrent was dramatically enhanced after ALD treatment: approximately 1.4 mA cm^{-2} of photocurrent was generated by the Mo/CZTS/CdS/AZO/TiO_2 photoelectrode at −0.2 V vs RHE, while a photocurrent of more than 0.80 mA cm^{-2} at 0 V vs RHE was obtained for the best performing sample (see Supporting Information, Figure S6). On average over multiple samples (5×), the photocurrent was 0.4 mA cm^{-2} at 0 V vs RHE, indicating more consistent performance with this method. Interestingly, after the ALD treatment, large cathodic photocurrent transients are observed upon illumination, and corresponding anodic transients are measured after the illumination is turned off. This suggests that charges are accumulating at one of the electrode interfaces due to a charge transfer barrier.[31] In addition, we note that the strong dark current present in the unprotected electrode (especially cathodic of −0.1 V vs RHE) was significantly reduced upon ALD treatment, which indicates electrochemical stabilization of the photoelectrode. To confirm this hypothesis, cyclic voltammetry was carried out to compare the electrochemical behavior of the simultaneously deposited photoelectrode before and after ALD treatment. The results (shown in Figure S7, Supporting Information) clearly confirm an effective stabilization of the photoelectrode, represented by a decrease in the current (attributed to corrosion) of almost 2 orders of magnitude throughout the potential window considered, under both dark and light conditions. Furthermore, visual inspection of the unprotected cells showed a marked change in the color after repeated cyclic voltammetry, while the appearance of the ALD protected cells remained unchanged (not shown).

Figure 4 also illustrates that another important point regarding the photoactivity of the CZTS electrodes was the necessity to employ the n-CdS layer to obtain reasonable photocurrent. Indeed, our attempt to prepare Mo/CZTS/AZO/TiO_2 electrodes resulted in samples with almost no observable photocurrent even under highly cathodic polarization (Figure 4, green curves). This was surprising considering that the AZO/TiO_2 combination has been shown to enhance charge extraction for Cu_2O electrodes, and even if a barrier is formed at the CZTS/AZO interface, it should still be possible to collect photogenerated charges with sufficient applied bias. Assuming that the CZTS is producing the photocurrent, and not the CdS or TiO_2, this result suggests that the interface between the AZO and the CZTS is a source of charge recombination (e.g., due to defects and/or trapping states), while the interfaces of CZTS/CdS and CdS/AZO are suitable for electron transfer.

To confirm that the observed photocurrent is not due to photons absorbed in the CdS or TiO_2 layers, a 610 nm cutoff filter was employed. About 50% of the original photocurrent remained even after removing photons with energy greater than 610 nm (See Figure S8, Supporting Information). This ratio is consistent with the distribution of solar photons available to CZTS (E_g = 1.4 eV) and the standard solar spectrum and suggests that the CdS or TiO_2 is minimally contributing to the photocurrent to water reduction. In order to better compare our results with previous reports of electrodeposited CZTS, we evaluated the incident-photon-to-current efficiency (IPCE) of top-performing simultaneously deposited electrodes using Eu^{3+} as an electron acceptor (Figure S9, Supporting Information). We found a maximum IPCE of around 10% at −0.4 V vs Ag/AgCl in 0.1 M Eu^{3+}, while the best results reported by Scragg et al.[25,32] are around 30% under similar conditions. Some photocurrent loss can be attributed to accumulation of charges at the interfaces as evidenced by the cathodic spikes discussed previously. On the other hand, our IPCE results further indicate that photocurrent originates from the CZTS as opposed to the CdS or TiO_2 as over 5% IPCE is observed at wavelengths greater than 600 nm.

In an effort to maximize the photocurrent produced by the cells, many different deposition conditions were attempted. As mentioned before, the irreproducible nature of the sequential deposition technique did not allow us to draw any significant insight into which deposition parameters lead to maximum photocurrent. However, the photocurrent of the simultaneously deposited samples showed a strong dependence on the voltage applied during the electrodeposition. These data are represented as the ratio of photocurrent to dark current as a function of the electrodeposition potential in the inset of Figure 4b. A very small window for high activity was seen. The photocurrent was close to zero at 1.2 and 1.1 V, but at 1.15 V, the photocurrent was found to be a maximum at over 6 times the magnitude of the dark current. This trend, although less pronounced, is identical for the unprotected Mo/CZTS/CdS electrodes, thus suggesting that the effect is due to differences in the composition of the material deposited at the different potentials. While it is known that the stoichiometry and especially the deficiency of copper is known to have a large effect on the photocurrent produced by CZTS for photovoltaic cells, the simultaneous approach does not allow for the individual tuning of the deposition rate (and thus the relative amounts in the films) of the copper, zinc, or tin. This is a drawback of the simultaneous deposition and presumably the reason for the high sensitivity of the photocurrent to the applied potential.

The stability of the photocurrent generated with and without the protective ALD coating was further evaluated by chronoamperometric measurements at 0 V vs RHE, carried out after linear sweep voltammetry. Figure 5a, top, shows the typical effect of ALD protection on the stability of the sequentially deposited photoelectrodes. Before the treatment, the photoactivity vanishes within less than 10 min, while after the ALD treatment, the photocurrent retains over 85% of its initial value after 5 min and over 55% of its initial value after 15 min (equivalent to 160 μA cm^{-2}).

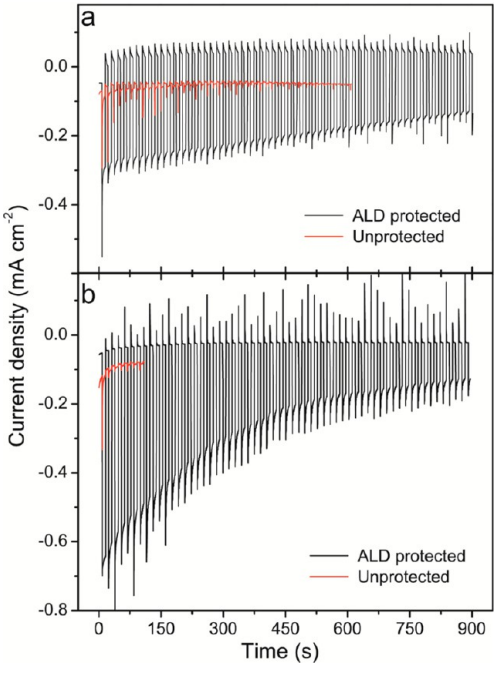

Figure 5. Chronoamperometric measurements at 0 V vs RHE under chopped light illumination for the sequentially (top) and simultaneously (bottom) deposited Mo/CZTS/CdS electrodes, with and without the ALD protective layer.

In Figure 5b, a similar effect is visible for the simultaneously deposited photoelectrodes: here again the photocurrent becomes vanishingly small within the first 5 min for the unprotected cell; on the contrary, the ALD-protected cells feature a much-improved activity and stability. In addition, we note that the drop in the photocurrent during chronoamperometric stability tests could be recovered to some extent by several means, such as by depositing an additional layer of platinum catalyst, by replacing the electrolyte solution with a fresh electrolyte and even by simple agitation of the electrolyte solution during the measurement. This clearly indicates that the gross results of chronoamperometric measurements are not indicative of the protected photoelectrode lifetime itself but are rather affected by other phenomena. While the recovery due to agitation and refreshing of the electrolyte solution allows us to attribute a part of the decrease in the current to mass-transfer limitations and bubble formation, the recovery upon deposition of an additional Pt catalyst layer indicates that the catalyst itself may become deactivated with time (due to poising by sulfur ions, for example). Increasing the photocurrent and stability by optimizing the HER catalysts and the protecting overlayers[33] are the important aspects to increase the viability of CZTS photocathodes for water reduction and should be the focus of future work. Moreover, following the latest advances with CZTS, it is reasonable to believe that the performances of such electrodes can be significantly further improved, for instance by incorporation of germanium[34] or by replacing molybdenum, which has been shown to lead to detrimental reactions with CZTS,[35] with an alternative back-contact material.

4. CONCLUSION

In conclusion, two recently reported electrodeposition routes toward CZTS thin film preparation have been investigated and compared for photoelectrochemical water splitting. The two methods lead to different properties and performances. In both cases, additional post-treatments, such as KCN etching and a CdS buffer layer, turned out to be highly beneficial for the performance of the photoelectrode. Despite our assumption that a sequential deposition would offer more ability to control the stoichiometry and the performance of the CZTS electrodes, the reproducibility turned out to be better using the simultaneous deposition route. Importantly, electrodes prepared via this route had not been used before to produce PEC cells for water reduction, and we report here a strong dependence of the photocurrent on the applied potential during electrodeposition. However, variability appeared to be quite significant for both deposition routes. Upon the preparation of dozens of electrodes, the photocurrent of the best and that of an average electrode differed by a factor of 2 or more. This variability, which was further exacerbated upon chemical bath deposition of the CdS buffer layer, appeared to be mitigated upon further deposition of a conformal protective coating by ALD technique. This fundamental step led to improved photoactivity and is attributed to further enhanced charge extraction, due to favorable interface formation with n-type ZnO and TiO_2. On top of that, the ALD coating dramatically enhanced the stability of the photoelectrode and made the study and characterization of the protected sample much more reliable. Owing to the deposition of a conformal, pinhole-free layer, the ALD protective strategy represents therefore a platform for easier optimization of the parameters

for manufacturing of otherwise unstable materials. By addressing the stability issues of CZTS-based photoelectrochemical cells, this work represents a further step toward viable CZTS-based water splitting and a step toward the long-term objective of fabricating CZTS-based photoelectrochemical devices that are capable of splitting water into hydrogen and oxygen with high efficiency and durability.

■ ASSOCIATED CONTENT

Supporting Information

Detailed experimental methods and Figures S1−S9 as described in the main text. This material is available free of charge via the Internet at http://pubs.acs.org.

■ AUTHOR INFORMATION

Corresponding Author

*E-mail: kevin.sivula@epfl.ch.

Notes

The authors declare no competing financial interest.

■ ACKNOWLEDGMENTS

L.R. and K.S. thank the EOS holdings S.A. (contract number 536067) and the FSB at EPFL for financial support. S.D.T. thanks the Swiss Federal Office for Energy (PECHouse Competence Center, contract number SI/500090-02) for financial support. We thank Prof. M. Stefik for assistance with Raman spectroscopy.

■ REFERENCES

(1) Service, R. F. *Science* **2004**, *305*, 958−961.
(2) Nozik, A. J.; Memming, R. *J. Phys. Chem.* **1996**, *100*, 13061−13078.
(3) Magnuson, A.; Styring, S. *Aust. J. Chem.* **2012**, *65*, 564−572.
(4) Walter, M. G.; Warren, E. L.; McKone, J. R.; Boettcher, S. W.; Mi, Q.; Santori, E. A.; Lewis, N. S. *Chem. Rev.* **2010**, *110*, 6446−6473.
(5) Brillet, J.; Yum, J. H.; Cornuz, M.; Hisatomi, T.; Solarska, R.; Augustynski, J.; Graetzel, M.; Sivula, K. *Nat. Photonics* **2012**, *6*, 824−828.
(6) Bolton, J. R.; Strickler, S. J.; Connolly, J. S. *Nature* **1985**, *316*, 495−500.
(7) Tachibana, Y.; Vayssieres, L.; Durrant, J. R. *Nat. Photonics* **2012**, *6*, 511−518.
(8) Seger, B.; Laursen, A. B.; Vesborg, P. C. K.; Pedersen, T.; Hansen, O.; Dahl, S.; Chorkendorff, I. *Angew. Chem., Int. Ed.* **2012**, *51*, 9128−9131.
(9) Boettcher, S. W.; Warren, E. L.; Putnam, M. C.; Santori, E. A.; Turner-Evans, D.; Kelzenberg, M. D.; Walter, M. G.; McKone, J. R.; Brunschwig, B. S.; Atwater, H. A.; Lewis, N. S. *J. Am. Chem. Soc.* **2011**, *133*, 1216−1219.
(10) Khaselev, O.; Turner, J. A. *Science* **1998**, *280*, 425−427.
(11) Paracchino, A.; Laporte, V.; Sivula, K.; Grätzel, M.; Thimsen, E. *Nat. Mater.* **2011**, *10*, 456−461.
(12) Sivula, K.; Le Formal, F.; Grätzel, M. *ChemSusChem* **2011**, *4*, 432−449.
(13) Ye, H.; Park, H. S.; Akhavan, V. A.; Goodfellow, B. W.; Panthani, M. G.; Korgel, B. A.; Bard, A. J. *J. Phys. Chem. C* **2011**, *115*, 234−240.
(14) Yokoyama, D.; Minegishi, T.; Maeda, K.; Katayama, M.; Kubota, J.; Yamada, A.; Konagai, M.; Domen, K. *Electrochem. Commun.* **2010**, *12*, 851−853.
(15) Ito, K.; Nakazawa, T. *Jpn. J. Appl. Phys.* **1988**, *27*, 2094−2097.
(16) Scragg, J. J.; Dale, P. J.; Peter, L. M.; Zoppi, G.; Forbes, I. *Phys. Status Solidi B* **2008**, *245*, 1772−1778.
(17) Pawar, S. M.; Pawar, B. S.; Moholkar, A. V.; Choi, D. S.; Yun, J. H.; Moon, J. H.; Kolekar, S. S.; Kim, J. H. *Electrochim. Acta* **2010**, *55*, 4057−4061.
(18) Kameyama, T.; Osaki, T.; Okazaki, K.-i.; Shibayama, T.; Kudo, A.; Kuwabata, S.; Torimoto, T. *J. Mater. Chem.* **2010**, *20*, 5319−5324.
(19) Riha, S. C.; Fredrick, S. J.; Sambur, J. B.; Liu, Y.; Prieto, A. L.; Parkinson, B. A. *ACS Appl. Mater. Interfaces* **2010**, *3*, 58−66.
(20) Yokoyama, D.; Minegishi, T.; Jimbo, K.; Hisatomi, T.; Ma, G.; Katayama, M.; Kubota, J.; Katagiri, H.; Domen, K. *Appl. Phys. Express* **2010**, *3*, 101202.
(21) Paracchino, A.; Mathews, N.; Hisatomi, T.; Stefik, M.; Tilley, S. D.; Gratzel, M. *Energy Environ. Sci.* **2012**, *5*, 8673−8681.
(22) Araki, H.; Kubo, Y.; Jimbo, K.; Maw, W. S.; Katagiri, H.; Yamazaki, M.; Oishi, K.; Takeuchi, A. *Phys. Status Solidi C* **2009**, *6*, 1266−1268.
(23) Ma, G.; Minegishi, T.; Yokoyama, D.; Kubota, J.; Domen, K. *Chem. Phys. Lett.* **2011**, *501*, 619−622.
(24) Todorov, T. K.; Reuter, K. B.; Mitzi, D. B. *Adv. Mater.* **2010**, *22*, E156−E159.
(25) Scragg, J. J.; Dale, P. J.; Peter, L. M.; Zoppi, G.; Forbes, I. *Phys. Status Solidi B* **2008**, *245*, 1772−1778.
(26) Fernandes, P. A.; Salomé, P. M. P.; da Cunha, A. F. *Thin Solid Films* **2009**, *517*, 2519−2523.
(27) Fontane, X.; Calvo-Barrio, L.; Izquierdo-Roca, V.; Saucedo, E.; Perez-Rodriguez, A.; Morante, J. R.; Berg, D. M.; Dale, P. J.; Siebentritt, S. *Appl. Phys. Lett.* **2011**, *98*, 181905−181903.
(28) Mitzi, D. B.; Gunawan, O.; Todorov, T. K.; Wang, K.; Guha, S. *Sol. Energy Mater. Sol. Cells* **2011**, *95*, 1421−1436.
(29) Scragg, J. J.; Wolverson, D.; Zoppi, G.; Peter, L. M. *Mater. Res. Soc. Symp. Proc.* **2009**, *1210*, DOI: 10.1557/PROC-1210-Q06-03.
(30) Scragg, J. J. *Copper Zinc Tin Sulfide Thin Films for Photovoltaics*; Springer: Berlin Heidelberg, 2011; ISBN: 978-3-642-22919-0.
(31) Le Formal, F.; Sivula, K.; Grätzel, M. *J. Phys. Chem. C* **2012**, *116*, 26707−26720.
(32) Scragg, J. J.; Dale, P. J.; Peter, L. M. *Electrochem. Commun.* **2008**, *10*, 639−642.
(33) Tilley, S. D.; Schreier, M.; Azevedo, J.; Stefik, M.; Graetzel, M. *Adv. Funct. Mater.* **2013**, DOI: 10.1002/adfm.201301106.
(34) Bag, S.; Gunawan, O.; Gokmen, T.; Zhu, Y.; Mitzi, D. B. *Chem. Mater.* **2012**, *24*, 4588−4593.
(35) Scragg, J. J.; Wätjen, J. T.; Edoff, M.; Ericson, T.; Kubart, T.; Platzer-Björkman, C. *J. Am. Chem. Soc.* **2012**, *134*, 19330−19333.